Atogami et al., *Cogent Medicine* (2016), 3: 1251833
http://dx.doi.org/10.1080/2331205X.2016.1251833

cogent medicine

HEMATOLOGY | RESEARCH ARTICLE

Red blood cell size differential method for time-series detailed monitoring of anemic disorders with RBC size abnormalities in mean corpuscular volume (MCV) and/or red blood cell distribution width (RDW)

Sunao Atogami[1,2*], Charles de Kerckhove[3], Katsunori Yanagihara[1] and Shimeru Kamihira[1,3]

Received: 01 September 2016
Accepted: 17 October 2016
First Published: 24 October 2016

*Corresponding author: Sunao Atogami, Department of Laboratory Medicine, Nagasaki University Graduate School of Biomedical Sciences, 1-7-1, Sakamoto, Nagasaki-shi, Nagasaki 852-8501, Japan; Department of Laboratory Medicine, Sasebo City General Hospital, 9-3, Hirase-cho, Sasebo-shi, Nagasaki 857-8511, Japan
E-mail: atogami@hospital.sasebo.nagasaki.jp

Reviewing editor:
Udo Schumacher, University Medical Center Hamburg-Eppendorf, Germany

Additional information is available at the end of the article

Abstract: *Background*: Size heterogeneity in red blood cells (RBCs), as indicated by elevated RBC distribution width (RDW), is increasingly considered a prognostic factor in various diseases. However, the semi-quantitative nature of the RDW value appears limited when evaluating quantitative changes in time-series RBC size distributions over a clinical course. *Methods*: We developed a time-series anemia monitoring program by displaying progressive differences between six size fractions in an RBC size distribution. To standardize each variation precisely, our program includes an angular transformation that is applied to all measured count ratio data. *Results*: By representing microcytic and/or macrocytic changes in time series independently, this method appears to improve evaluations of anisocytosis, reflecting the responsiveness of treatments and effects, such as deficiencies in iron or vitamin B12. Time-series displays of RBC size changes also appear to enable verification of latent clinical developments at earlier stages and the characterization of imbalances between RBC supply and RBC loss in anemic pathologies. *Conclusions*: By displaying linear relationships between RBC size categories on a time scale, our proposed

ABOUT THE AUTHORS

Sunao Atogami's interest in a parametric analysis method by flow cytometry-measured histograms in time series came from past research of DNA aneuploidy changes in adult T-cell leukemia cells, over the course of monitoring ATL patients under the direction of Nagasaki University professor Emeritus Shimeru Kamihira. His research currently focuses on applying the same parametric analysis to a monitoring method of anisocytosis or elevated RBC distribution width (RDW), a more common clinical finding which relates to the various pathogeneses of anemic disorders as apparent in time series.

Charles de Kerckhove is a Mechanical Engineer keen to build on the Engineering approach and related distant memories of Statistics for a thorough understanding and communication of how to display hematological change in time series.

Katsunori Yanagihara, professor at Nagasaki University and Head of the Nagasaki University Hospital Department of Laboratory Medicine, and Shimeru Kamihira are both supervisors of this study.

PUBLIC INTEREST STATEMENT

Flow cytometry count data, such as complete blood cell counts, have been widely used in clinical laboratories. We usually must use non-parametric statistical analysis to compare such cell count data, but quantitative evaluations employing some type of computed index from count data in time series can at times be necessary for making key clinical decisions. Therefore, we studied the characteristics of both precision and accuracy and the instability of uncertainty in count ratio variables for improved clarity in flow cytometry analysis. Through our proposed control of uncertainty propagation in computed indices from a hematology analyzer's cell count data, we hope that our clinical evaluation method might contribute to an easy-to-visualize, programmable, and real-time detailed anemia interface. We also hope that our report's case studies on tracking various types of anemia might indicate such a method's potential applicability to routine medical care.

monitoring method quantifies potentially applicable pathological information. This mode of representation appears to offer details about high RDW values and latent adverse outcomes related to anemic pathogenesis.

Subjects: Computer Graphics & Visualization; Hematology; Medical Statistics & Computing

Keywords: anemia monitoring; flow cytometry; measurement uncertainty; MCV; RDW

1. Introduction

In a complete blood cell count (CBC), performed as a routine laboratory test in anemia diagnosis, a hematology analyzer measures the volume of each erythrocyte to create a histogram of cell size distribution. This probability distribution provides two main output parameters: the mean corpuscular volume (MCV), which is the mean value of the distribution, and the red blood cell distribution width (RDW), which represents the degree of dispersion in the distribution (Kachel, 1982; Tatsumi et al., 1999). Recently, elevated RDW has been investigated as a predictor of mortality in various non-hematological disorders, such as inflammation and circulatory diseases (Cauthen, Tong, Jain, & Tang, 2012; Hu et al., 2013; Lippi & Plebani, 2014; Montagnana, Cervellin, Meschi, & Lippi, 2012). However, when interpreting central values, such as MCV and RDW, in time series, it can be difficult to evaluate information about cellular volume changes with minimal or latent anisocytosis in the red blood cell (RBC) size distribution.

Accordingly, we established a new evaluation method called "RBC size differentials", which enables time-series partial analysis of RBC size distribution derived from a hematology analyzer without additional cost. Using data from daily control checks for counting RBCs and white blood cells (WBCs), we investigated the measurement uncertainty of our flow cytometric approach and verified the reliability of our computed indices obtained from RBC size differential methods.

2. Methods

2.1. Data collection

To examine CBC data, including MCV and RDW indices, we used an XE-5000 hematology analyzer (a recent model; Sysmex Corp., Kobe, Japan) at Sasebo City General Hospital from June 2013 to May 2016 and an SF-3000 (a past model; Sysmex Corp., Kobe, Japan) at Nagasaki Harbor Medical Center Community Hospital from July 1998 to September 2005 for a pilot study. This study's data were acquired through standard blood test procedures with daily quality control checks. Data from 307,246 clinical samples data from the XE-5000 analyzer and 5,087 clinical samples from the SF-3000 analyzer were registered in our database for RBC size differentials.

To obtain the probability distributions of RBC size, PNG-format digital images were first output from the XE-5000 analyzer. Next, the images were converted to numerical form by subdividing the x-axis into 256 points for compilation in a relational database. Alignment of the x-axis relative to the origin was confirmed by statistically comparing the cumulative mean value of RBC size to the cumulative analyzer's MCV data (for details, see Appendix 1 and Figure A1). Using the same approach, the printed image data of RBC size distributions from the SF-3000 analyzer were manually digitized in another database. When comparing MCV values for a single given probability distribution, values from relational databases were observed to be consistent with MCV values from the hematology analyzer output.

2.2. RBC size differential method

2.2.1. Establishing six RBC size fractions (Step 1)

Ranging between extreme limits of 41–160 fL, RBC size distributions were fractionized into the following six size fractions every 20 fL, called "RBC size differentials", as shown in the RBC size

cogent medicine

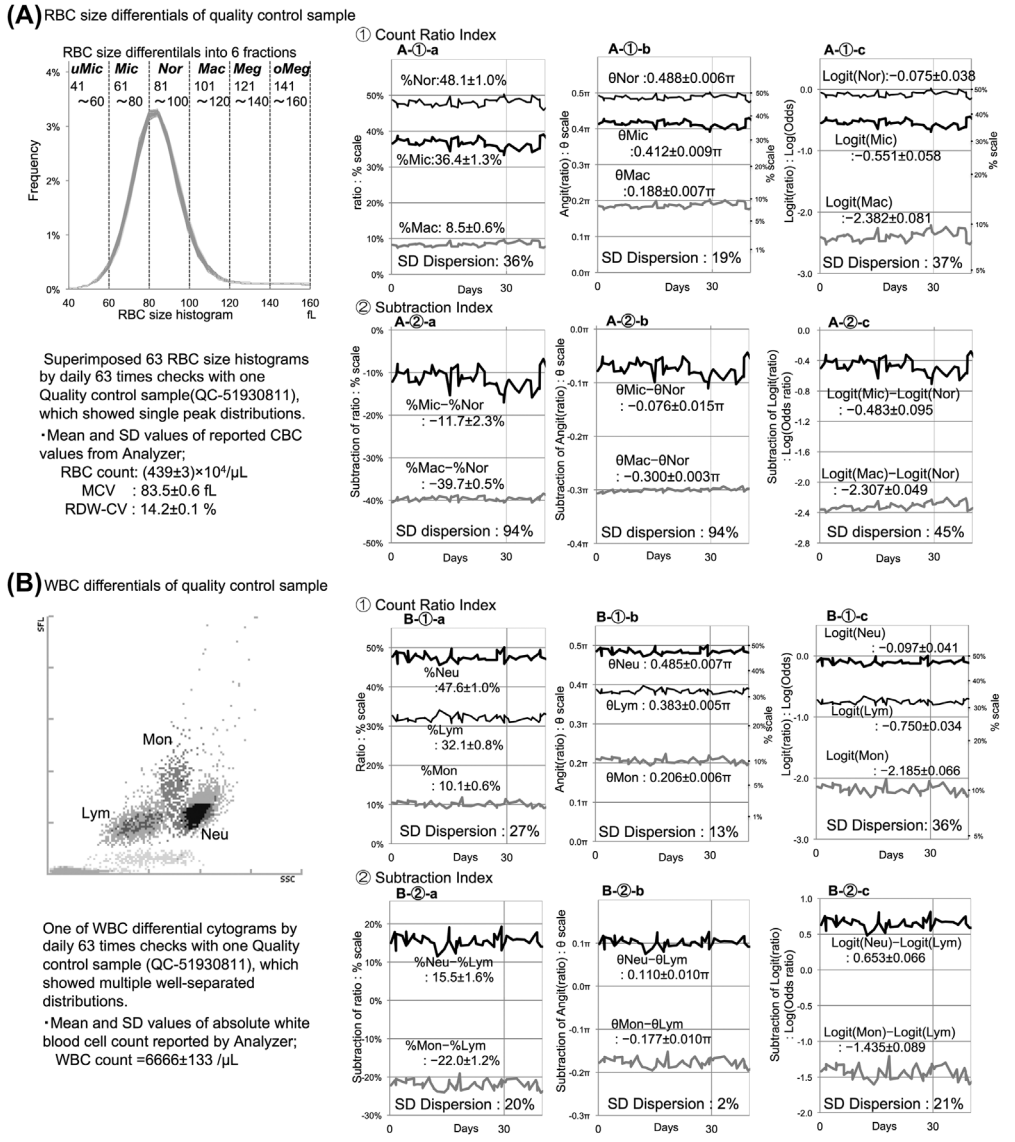

Figure 1. Evaluation of measurement uncertainty in the blood cell differential method.

Notes: We evaluated the error-stabilizing effects of the *Angit*(p) and Logit(p) functions according to the degree of SD dispersion, which is the coefficient of variation (CV%) of each fluctuation's standard deviation (SD) variable. The *Angit*(p) function standardized uncertainty most effectively in the count ratio index because of its smaller SD dispersion. However, the uncertainty-stabilizing effects in the subtraction index revealed a discrepancy between the RBC size differentials and WBC differentials (A-2-b:94% vs. B-2-b:2%). Furthermore, a synchronized fluctuation pattern with a mirror image and parallel image in the count ratio index was observed only in the RBC size differentials, which might amplify and offset the uncertainty in the subtraction index, as shown in the A-2 series graphs. All 76 courses of quality control checking were analyzed similarly and are summarized in Table 1.

distribution in Figure 1: under-microcytic (uMic), microcytic (Mic), normocytic (Nor), macrocytic (Mac), megalocytic (Meg), and over-megalocytic (oMeg).

2.2.2. Computing the count ratio p of each RBC size fraction (Step 2)

Using the relational database, we computed the count ratio p as the percentage of each fraction's area under the curve within the 41–160 fL RBC size distribution. The six count ratios' values of p corresponding to each of the respective fractions were labeled %uMic, %Mic, %Nor, %Mac, %Meg, and %oMeg.

2.2.3. Transforming the count ratio p variable to angle ratio θ to standardize precision (Step 3)

Because our method for representing true change requires the calculation of differences, variations in precision among the six fractions must be standardized. Subjecting the count ratio p data to a variance-stabilizing transformation (Kirk, 2013) resulted in distributions with a standard deviation (SD) value independent of the p variable. This angular transformation is a function defined as $\theta(p) = 2 \cdot \arcsin\sqrt{p}$, which we called *Angit*(p). The mean values of the transformed six angle ratio θs are then subtracted from one another, thus reducing disparities in precision. Corresponding to the fractions identified in Step 2, the angle ratio θs were called θuMic, θMic, θNor, θMac, θMeg, and θoMeg.

2.2.4. Establishing RBC size differential indices (Step 4)

The six angle ratio θs were utilized alone as each RBC size differential index, with equal precision in theory. Furthermore, two additional RBC size differential indices were established by subtracting the θNor value from the θMic and θMac values. Respectively called [θMic–θNor] and [θMac–θNor] with equal precision in theory (Taylor, 1997), these indices reflect the difference in each RBC size fraction relative to the central Nor-fraction.

2.3. Measurement uncertainty in flow cytometric count data for blood cell differentials

We evaluated measurement uncertainty in our blood cell differential method with data from daily quality control checks based on the notion that the fluctuation in repeated measurements of the same sample should reflect the measurement uncertainty.

We compared the differences in the uncertainty in differential indices between the RBC size differentials and WBC differentials. Using statistical analyses with 38 courses of two different series of quality control checks with different cell concentrations by the XE-5000 analyzer, we investigated the uncertainty-stabilizing effects of both angular transformation and *Logit* transformation on both the count ratio index and the subtraction index, according to the degree of the fluctuation's dispersion based on each index's SD, which is closely reflective of precision in general. The additional coefficient of variation of these SD values, which we called "SD dispersion", was calculated as (standard deviation of SD values/mean of SD values) × 100. For our rationale for applying the *Angit*(p) and *Logit*(p) functions, see Appendices 2 and 3.

2.4. Cut-off values of RBC size differential indices evaluated by receiver operating characteristic (ROC) curve analysis

Reference intervals of MCV and RDW were determined by satisfying the following clinically accepted criteria for normal RBC volume conditions: (1) an MCV from 80 to 100 fL (or 10^{-15}L) (Sacher, McPherson, & Campos, 1991); and (2) an RDW-CV < 16%. RDW-CV was calculated as (standard deviation of mean corpuscular volume/mean corpuscular volume) × 100. A cut-off of 16% was identified as the upper limit of a normal sample (Rezende, Lijfering, Rosendaal, & Cannegieter, 2014). We evaluated the count ratio indices of θMic, θMic and θMac and the subtraction indices of [θMic–θNor] and [θMac–θNor] as the discriminators for RBC size abnormality according to the clinical criteria for MCV and RDW values: normocytosis ($80 \leqq MCV \leqq 100$ and RDW-CV < 16%), microcytosis (MCV < 80 fL), macrocytosis (MCV > 100 fL) and normal range of RDW (RDW-CV < 16%). We determined the optimal cut-off values based on the method using the Youden index by ROC analysis (Hajian-Tilaki, 2013) with 307,246 CBC samples from the XE-5000 analyzer and 5,087 samples of patients with hematological disorders from the SF-3000 analyzer. Then, we compared the cut-off points between the two hematology analyzers: a recent model and past model manufactured prior to sheath-flow method integration (Tatsumi et al., 1999). ROC analysis was performed by statistical computing, using R software via http://www.R-project.org (The R Project for Statistical Computing, Vienna, Austria).

2.5. Graph preparation for visualizing the changes in time-series CBC data

The clinical courses of all anemic patients with RBC size abnormalities or RDW elevation were evaluated using our CBC time-series graph preparation program. For Cases 1–5, we compared similarities and differences in graph patterns among patients of differing pathologies by means of RBC size differentials, superimposed RBC size distributions and other CBC data while considering hidden measurement uncertainty in RBC size differential indices. All numerical computations and graphs for this study were conducted using Microsoft Excel software.

2.6. Ethics

This study was approved by the Institutional Review Board of Nagasaki Harbor Medical Center Community Hospital and Sasebo City General Hospital and was conducted in accordance with the ethical principles of the Declaration of Helsinki. Its communication is consistent with the Code of Ethics of the American Medical Writers Association.

3. Results

3.1. Characteristics of measurement uncertainty in blood cell differential methods (Figure 1 and Table 1)

Figure 1 shows the fluctuation patterns of measurement uncertainty in each differential index: (1) Count ratio index and (2) Subtraction index in both methods of (A) RBC size differentials and (B) WBC differentials. Non-transformed differential indices are shown in the graphs at left (a-series), transformed indices by *Angit* function in the middle graphs (b-series), and transformed indices by *Logit* function in the graphs at right (c-series). The statistical values of mean ± standard deviation in each index are noted at the positions of the corresponding lines, and computed SD dispersions (CV%) are noted at the bottom of each graph. All SD values and SD dispersion values from the total of 76 courses of quality control checks are analyzed statistically in Table 1.

First, the angular transformation by *Angit* function standardized the uncertainty most effectively in the count ratio index, according to the smallest SD dispersion; however, the uncertainty in the subtraction index exhibited an obvious discrepancy between RBC size differentials and WBC differentials. Next, there were typical graphical findings of synchronized patterns in the fluctuations in the count ratio index, revealing both reciprocal mirror and parallel images between side-by-side fractions, which caused the amplification and offset of fluctuation in the subtraction index only in RBC size differentials. Because the statistical comparison of SD values in the transformed count ratio index by *Angit* function revealed no difference between RBC size differentials vs. WBC differentials (A-1-b vs. B-1-b in Figure 1 and Table 1), we speculated that this discrepancy in the subtraction index might be caused by uncertainty other than precision, which was already equalized in the count ratio index.

3.2. Cut-off points of each RBC size differential index (Table 2)

ROC analysis indicated that for both hematology analyzers, θNor, θMic and θMac might be good discriminators of normocytosis, microcytosis and macrocytosis, respectively. Furthermore, because the cut-off point of the [θMic–θNor] index was exactly 0.00π for both analyzers, microcytosis of MCV < 80 fL might correspond to the same distributions as the microcytic state of [θMic–θNor] > 0 for both analyzers. By contrast, for judgment of the macrocytic state, the cut-off point of the [θMac–θNor] index was −0.02π for the XE-5000 analyzer and −0.05π for the SF-3000 analyzer. These different shifts in cut-off point from 0.00π might depend on their skewness to the left in the RBC size distributions based on the mechanical difference in analyzers with or without sheath-flow methods (Tatsumi et al., 1999). However, the [θMic–θNor] and [θMac–θNor] indices might be good indicators of hematological microcytosis and macrocytosis, respectively, based on their high AUC% values.

3.3. How this method facilitates the visualization of states of size abnormality: Displaying multi-variable time series

Figures 2–4 show how the RBC volume differential time series might complement MCV and RDW indicators to improve the pathological diagnosis of various anemic disorders. The x-axis in days is common to all time-series graphs, and the following indices are represented by the y-axes in the four time-series partitions from top to bottom: (1) hemoglobin (HGB) on the main y-axis and hematocrit (HCT) on the second y-axis; (2) MCV on the main y-axis and RDW-CV% on the second y-axis; (3) angle ratio θ (π) on the main y-axis (linear scale) and its original count ratio p (%) on the second y-axis (non-linear scale); and (4) RBC size indices. At the bottom, the superimposed RBC size distributions from the analyzer indicate partial qualitative changes (labeled “Frequency” for “Frequency distribution graph”). All the following cases appear to indicate relative RBC size fractional changes for specific time periods according to varying pathologies.

3.4. Assessing time-series RBC size changes associated with erythroid maturation disorders (Figure 2)

In Case 1, before vs. after TS-1 chemotherapy for a lung cancer patient (typical case), and in Case 2, before vs. after an allogeneic bone marrow transplant with RBC transfusions for a severe aplastic anemia patient

In Case 1, there were a few spikes in the [θMac−θNor] line (marked with arrows) in accordance with drip infusion therapies, which might have been deviations due to possible unexpected uncertainty propagation. Although the megalocytic fraction was stable after chemotherapies with CBDCA, PTX and BV, the increasing megalocytic trend with a complementary normocytic decrease immediately before Day 257 suggested DNA synthesis inhibitor effects due to disruption of erythroid maturation by TS-1.

In Case 2, two time points of macrocytic states with high-level megalocytic fractions seemingly derived from pathological erythroid clones with maturation disorder gradually disappear due to conditioning regimens, and the prominent microcytic increase might reflect RBC supply from transfusions. After Day 89, normocytic and macrocytic increases without a macrocytic state appear to indicate normal erythroid recovery derived from transplanted stem cells, and the concurrent microcytic decrease suggests rapid removal of older transfused RBCs from the peripheral blood.

3.5. Assessing time-series RBC size distributions for pathological abnormalities related to disseminated intravascular coagulation (DIC), with potentially shortened RBC lifespan (Figure 3)

In Case 3, caused by massive vascular bleeding, and in Case 4, caused by extravascular hemolysis with findings of RBC fragmentation.

In Case 3, the increase and subsequent decrease in the megalocytic fraction mirror the decrease and subsequent increase in the normocytic fraction; these transitions appear to reflect marrow responses to severe anemia caused by bleeding. Case 4 offers an interesting comparison because the normocytic and macrocytic increases appear to reflect marrow responses to severe anemia caused by hemolysis with RBC fragmentation, as indicated by the leftward shift of the frequency distribution graph. In both cases, the transient megalocytic increase might be a similar basic pattern of reaction to severe anemia, except for the brief presence of a microcytic state in Case 4.

3.6. Assessing changing microcytic states caused by iron deficiency in different clinical backgrounds (Figure 4)

In Case 5, showing a typical recovery course with ferric therapy, in contrast to Case 6, showing retardation in anemia recovery due to massive menstrual bleeding for one week, and Case 7, showing the common complication of iron deficiency during vitamin B12 treatment.

Cases 5 and 6 both exhibited a decreasing [θMic-θNor] line and similar durations of a microcytic state (θMic > θNor). However, only Case 6 exhibited an additional macrocytic increase with a macrocytic state (θMac + 0.05π > θNor) and a bimodal pattern in the RBC volume distribution, which might be a transient response of excessive erythropoiesis to massive bleeding. In Case 7, concurrent with a decreasing [θMac-θNor] and θMeg, an upward trend in the [θMic−θNor] line and a subsequent microcytic state were observed. Because this [θMic−θNor] index increase appears to indicate the extent of iron deficiency, this time-series may help guide the timing or decision for ferric medicine treatment–specifically, one week earlier than conducted for Case 7.

3.7. Assessing fractional rebalancing between RBC supply and RBC loss (Figures 2 and 3)

In our view, RBC size differential methods in time series have the potential to quantify each fraction's change rates in the RBC size distribution. Although the superimposed RBC size distributions of Cases 1 and 3 merely present similar increases in the megalocytic fraction, the RBC size differentials

Table 1. Statistics for the evaluation of measurement uncertainty in flow cytometric differential data

(a) RBC size differentials of quality control samples

RBC size differential index			Checks with QC****0810 series (*n* = 38) RBC count: (234 ± 2)×10⁴/μL MCV: 76.5 ± 1.9 fL RDW-CV: 16.2 ± 1.0%				Checks with QC****0811 series (*n* = 38) RBC count: (441 ± 3)×10⁴/μL MCV: 83.1 ± 1.2 fL RDW-CV: 14.5 ± 0.3%			
			SD value		SD dispersion		SD value		SD dispersion	
			Mean	±SD	Mean (%)	±SD (%)	Mean	±SD	Mean (%)	±SD (%)
1. Count ratio index	a	%Mic	0.9%	±0.3%	64*	±11	1.5%	±0.4%	41*	±3
		%Nor	1.3%	±0.3%			1.1%	±0.3%		
		%Mac	0.3%	±0.1%			0.7%	±0.2%		
	b	*Angit*(Mic):θMic	0.006π	±0.002π	37*	±15	0.010π	±0.003π	22*	±4
		Angit(Nor):θNor	0.009π	±0.002π			0.007π	±0.002π		
		Angit(Mac):θMac	0.005π	±0.001π			0.008π	±0.002π		
	c	Logit(Mic)	0.038	±0.014	39	±13	0.066	±0.017	33	±6
		Logit(Nor)	0.063	±0.018			0.044	±0.013		
		Logit(Mac)	0.079	±0.015			0.086	±0.020		
2. Subtraction index	a	%Mic−%Nor	2.2%	±0.7%	48	±11	2.6%	±0.7%	93	±10
		%Mac−%Nor	1.1%	±0.3%			0.5%	±0.2%		
	b	[θMic−θNor]	0.015π	±0.004π	61	±15	0.017π	±0.005π	99	±10
		[θMac−θNor]	0.006π	±0.002π			0.003π	±0.001π		
	c**	Logit(Mic)−Logit(Nor)	0.099	±0.027	50	±18	0.109	±0.029	55	±11
		Logit(Mac)−Logit(Nor)	0.046	±0.008			0.047	±0.010		

(b) WBC differentials of quality control samples

WBC differential index			Tests with QC****0810 series (*n* = 38) WBC count: 2921 ± 67/μL				Tests with QC****0811 series (*n* = 38) WBC count: 6646 ± 120/μL			
			SD value		SD dispersion		SD value		SD dispersion	
			Mean	±SD	Mean (%)	±SD	Mean	±SD	Mean (%)	±SD
1. Count ratio index	a	%Neu	1.2%	±0.1%	19*	±6	1.0%	±0.1%	24*	±6
		%Lym	1.3%	±0.2%			0.8%	±0.1%		
		%Mon	0.9%	±0.1%			0.7%	±0.1%		
	b	*Angit*(Neu):θNeu	0.008π	±0.001π	11*	±5	0.007π	±0.001π	13*	±6
		Angit(Lym):θLym	0.009π	±0.001π			0.006π	±0.001π		
		Angit(Mon):θMon	0.009π	±0.001π			0.007π	±0.001π		
	c	Logit(Neu)	0.051	±0.005	38	±7	0.042	±0.004	39	±9
		Logit(Lym)	0.056	±0.007			0.038	±0.004		
		Logit(Mon)	0.098	±0.012			0.074	±0.011		
2. Subtraction index	a	%Neu−%Lym	2.3%	±0.2%	14	±8	1.6%	±0.2%	16	±8
		%Mon−%Lym	1.9%	±0.3%			1.3%	±0.1%		
	b	[θMic−θNor]	0.015π	±0.001π	6	±5	0.010π	±0.001π	6	±5
		[θMac−θNor]	0.015π	±0.002π			0.011π	±0.001π		
	c**	Logit(Neu)−Logit(Lym)	0.096	±0.010	22	±8	0.067	±0.007	25	±9
		Logit(Mon)−Logit(Lym)	0.132	±0.018			0.097	±0.012		

Notes: The measurement uncertainty in flow cytometric RBC and WBC count data was evaluated with 38 courses of two different series of quality control checks by an XE-5000 analyzer. This statistical summary verified that the *Angit*(p) function standardized measurement uncertainty in the count ratio index most effectively for both RBC size differentials and WBC differentials. Next, the discrepancy in the subtraction index shown in Figure 1 was confirmed statistically and might be derived from the propagation of some type of uncertainty other than precision. We guessed that the instability of accuracy in the count ratio index, which would amplify or offset the uncertainty propagation in the calculated subtraction index, might occur easily in our RBC size differentials method due to fixed gating.

*Statistical significance was verified with Wilcoxon signed-rank test.

**Subtraction of Logit(ratio) equals Log(Odds ratio).

Table 2. Cut-off points and %AUC (area under the curve) values of each RBC size differential index to discriminate abnormal states in RBC size distributions

Criteria (sample ratio)	RBC size differential index				
	θMic	θNor	θMac	[θMic−θNor]	[θMac−θNor]
XE-5000 analyzer					
Normocytosis or not (26:10)	–	0.48π (96.6%)	–	–	–
Microcytosis or not (10:131)	0.40π (99.1%)	–	–	0.00π (99.8%)	–
Macrocytosis or not (10:147)	–	–	0.41π (97.2%)	–	−0.02π (99.5%)
RDW < 16% or not (42:10)	–	0.49π (89.4%)	–	–	–
Total sample number = 307,246					
SF-3000 analyzer					
Normocytosis or not (10:17)	–	0.43π (96.6%)	–	–	–
Microcytosis or not (10:289)	0.38π (98.9%)	–	–	0.00π (99.8%)	–
Macrocytosis or not (10:19)	–	–	0.35π (93.9%)	–	−0.05π (98.4%)
RDW < 16% or not (10:12)	–	0.42π (84.4%)	–	–	–
Total sample number = 5,087					

Notes: Values at top of each cell show cut-off points; Values at bottom within brackets show %AUC.
Relationships between the indices of RBC size differentials and four criteria for diagnostic RBC conditions: normocytosis (80 ≦ MCV ≦ 100 and RDW-CV < 16%), microcytosis (MCV < 80 fL), macrocytosis (MCV > 100 fL) and the normal range of RDW (RDW-CV < 16%) were evaluated by ROC (receiver operating characteristic) analysis of 307,246 CBC samples on the XE-5000 analyzer and 5,087 samples of patients with hematological disorders using the SF-3000 analyzer. The differential indices of θNor, θMic and θMac showed high AUC% values, which might indicate good discrimination of normocytosis, microcytosis and macrocytosis, respectively. Furthermore, the [θMic-θNor] index with a cut-off point of 0.00π might be a meaningful indicator of microcytosis due to the microcytic state of only "θMic > θNor". By contrast, although the cut-off point shift from 0.00π in the [θMac-θNor] index might reflect the degree of skewness to the left in the RBC size distributions in both analyses, the [θMac-θNor] index might also be an indicator of macrocytosis because of the macrocytic state of nearly "θMac > θNor".

indicate that the increase in the θMeg line from 0.10 to 0.20π required approximately one month in Case 1 but only 10 days in Case 3. Similarly, the durations of the notable microcytic states were 32 days in Case 2 but only 8 days in Case 4.

These differences in the change rate with respect to the time scale might be attributable to differences in pathogenesis and the peripheral relative rebalancing between RBC supply (including transfusion) and RBC destruction or loss.

4. Discussion

4.1. Clinical significance of RBC size distribution and their variation with time

With the common application of MCV and RDW in treating anemia, RBC size has been shown to be a useful property for diagnosing pathological erythropoiesis. These indicators are directly affected by the heterogeneity of peripheral RBC populations at any given time because considerable variation has been noted beyond the mean RBC lifespan of approximately 115 days (Cohen et al., 2008; Franco, 2012), which is longer than the lifespans of other blood cells. Therefore, the RBC size distribution is often composed of heterogeneous RBC populations with differing maturation processes and differing ages from enucleation to destruction (Erslev & Beutler, 1995; Quigley et al., 2014). Because partial changes in RBC size distribution can reflect shifts in this balance between RBC supply and RBC age, this approach with trend analyses might improve the understanding of pathogenic

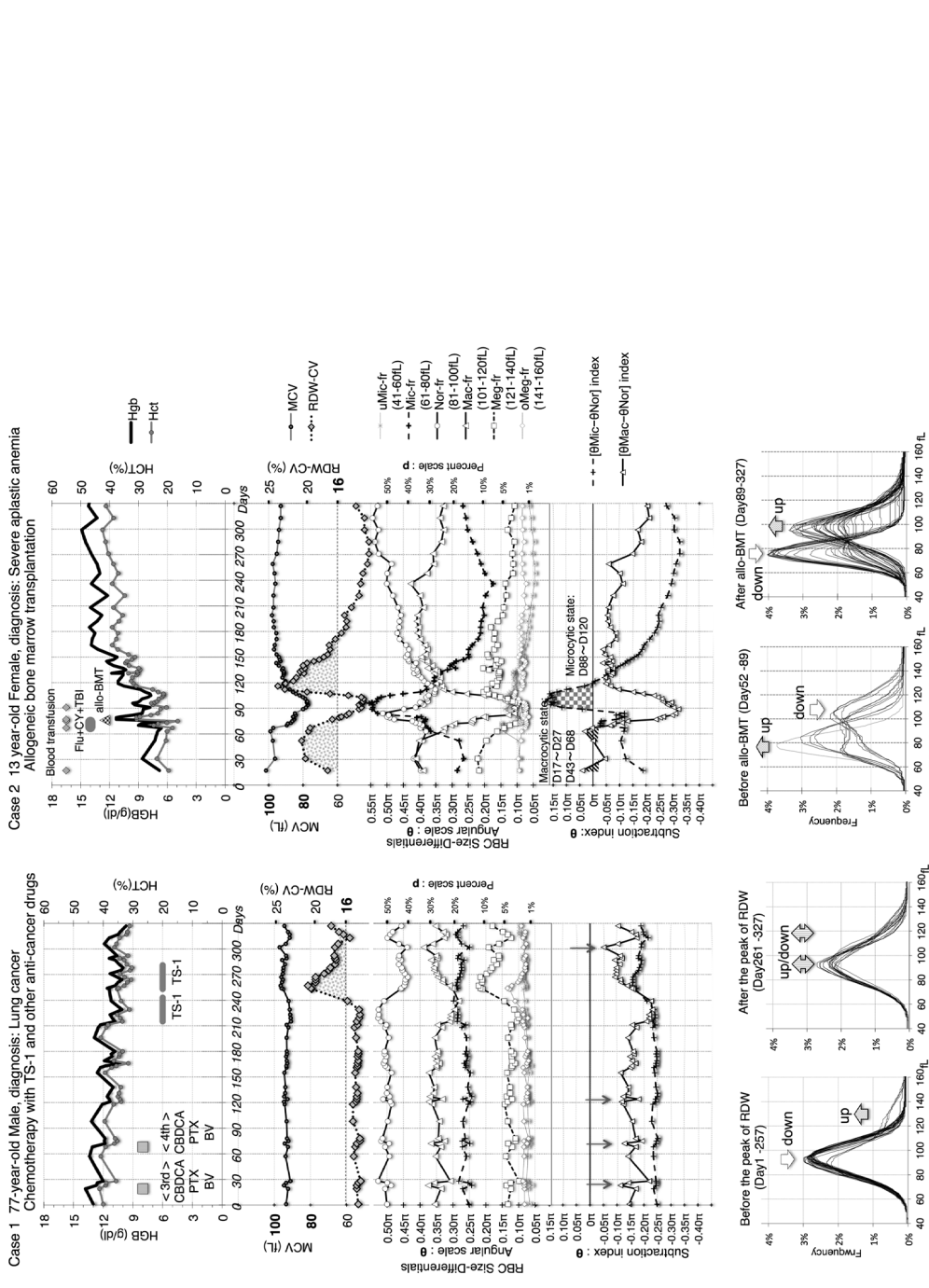

Figure 2. Time-series investigation of erythroid maturation disorders using the XE-5000 analyzer.

Notes: linical problem: To identify macrocytic RBC changes associated with erythroid maturation disorders and the recovery phase from marrow suppression using time-series data. Main relevant results from superimposed RBC size distributions: ["-fr"="fraction"].Case 1: From Day 1 to 257, Meg-fr increased, whereas Nor-fr decreased; from Day 261 to 330, Nor-fr, Mac-fr and Meg-fr fluctuated widely. Case 2: From Day 52 to 89, conditioning decreased the increased Mac-fr, and Mic-fr (reflecting transfused RBCs) increased to a peak value; from Day 89 to 327, Mac-fr and Nor-fr increased, whereas the peak in Mic-fr diminished. Inferred clinical significance of time-series differential indices: The effects of the DNA synthesis inhibitor (TS-1) medication were more evident in θMeg than in θMac without an overt macrocytic state of [θMac−θNor] > −0.02π in Case 1, whereas RBC immaturity appeared as two separate instances of the macrocytic state before BMT in Case 2. Additionally, there were a transient remarkable peak of the microcytic state of [θMic−θNor] > 0π and subsequent mild elevation in the [θMac−θNor] index after BMT in Case 2 (areas greater than the cut-off point are shaded.) The turning points of true changes in RBC size distribution related to clinical events such as chemotherapy and blood transfusion were visualized in graphs and were recognized easily. The spike-like changes observed in the [θMac−θNor] index, as indicated by down arrows in Case 1, might be considered amplified propagation of systematic error because of the presence of synchronized patterns in the RBC size differential graph, which might be induced by the minimal RBC size modification in vitro associated with drip infusion therapies, as shown in Figure 1.

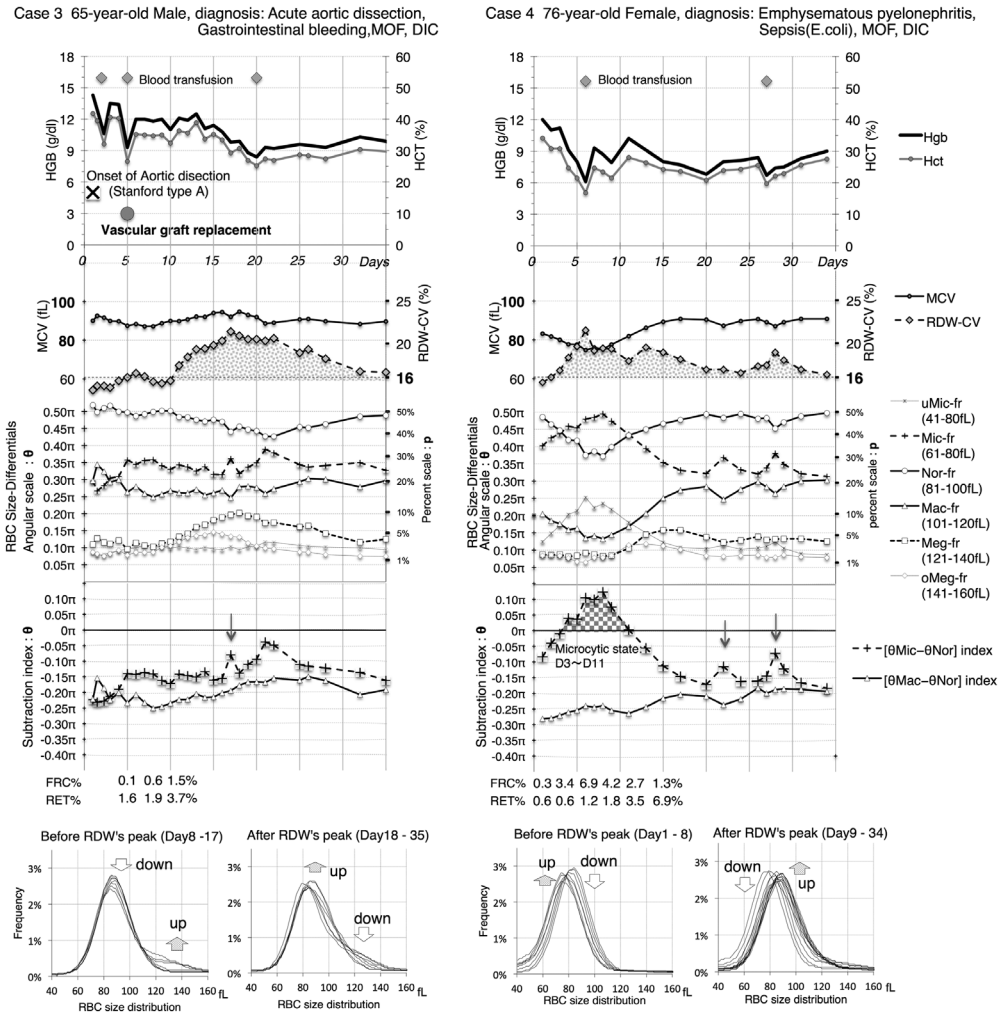

Figure 3. Notes: Time-series investigation of anemic pathogenesis in disseminated intravascular coagulation (DIC) using the XE-5000 analyzer.

Clinical problem: The patients in both cases developed DIC from different pathologies, but their anemias were similar and seemed likely related to shortened RBC lifespan due to massive bleeding in Case 3 and extra vascular hemolysis in Case 4. Main Relevant Results from Superimposed RBC Size Distributions: ["-fr"="fraction"]. Case 3: From Day 8 to 17, Meg-fr increased, whereas Nor-fr decreased; from Day 18 to 35, Nor-fr increased, and Meg-fr decreased. Case 4: From Day 1 to 8, uMic-fr and Mic-fr increased, whereas Nor-fr decreased; from Day 9 to 34, Nor-fr and Mac-fr increased, and uMic-fr and Mic-fr decreased conversely. Inferred clinical significance of time-series differential indices: The RDW elevations can be explained by an increase in the θMeg index in Case 3, which suggests an early response of erythropoiesis to severe anemia. By contrast, the early presence of the microcytic state of [θMic−θNor] > 0π and subsequent increase in θMeg index might underlie the RDW elevation in Case 4. This short microcytic state in Case 4 may suggest RBC fragmentation concurrent with blood transfusion because of the appearance of helmet cells in blood smear tests in Case 4 but not in Case 3. The down arrows in the [θMic-θNor] index in both cases suggest potential instability of the accuracy, except for the second arrow in Case 4, which was associated with blood transfusion.

developments affecting background anemic disorders, e.g. various RBC maturation abnormalities or RBC destruction/loss due to hemolysis or bleeding.

4.2. Prerequisite condition for time-series RBC size differential analysis

According to *measurement error theory* as concerns least-squares fitting (Taylor, 1997), a straight line drawn between two measured values requires the stability of the y-axis precision to be comparable to that of the x-axis of time. Therefore, in considering our variance-stabilizing transformation for standardizing the random error of all measured count ratio values, we emphasized our objective of time-series differences and not improving the measurement precision itself. The adoption of our semi-*Angit*(p) plot, which was derived to compare time-series cell differential indices based on flow cytometric count data, shares similarities with certain other approaches. For example, in real-time PCR (polymerase chain reaction) measurement procedures, including the serial dilution method, semi-logarithmic graphs are necessary for calibration curves. For our rationale for applying *Angit*(p) instead of the more widespread *Logit*(p) function, see Appendices 2 and 3 and the supporting statistical analyses in Table 1. The linear semi-*Angit*(p) plotting time-series graphs are necessary to attain our objective of linearized statistical analyses in detail, as applied in Figures 2–4.

4.3. Potential isolation of clear clinical trends and hidden systematic error

By indicating substantial relative changes within heterogeneous RBC populations, potentially also quantitatively, time-series RBC size differentials might support the identification of clear pathological trends. Our assumption, based on measurement error theory (Taylor, 1997), suggests that

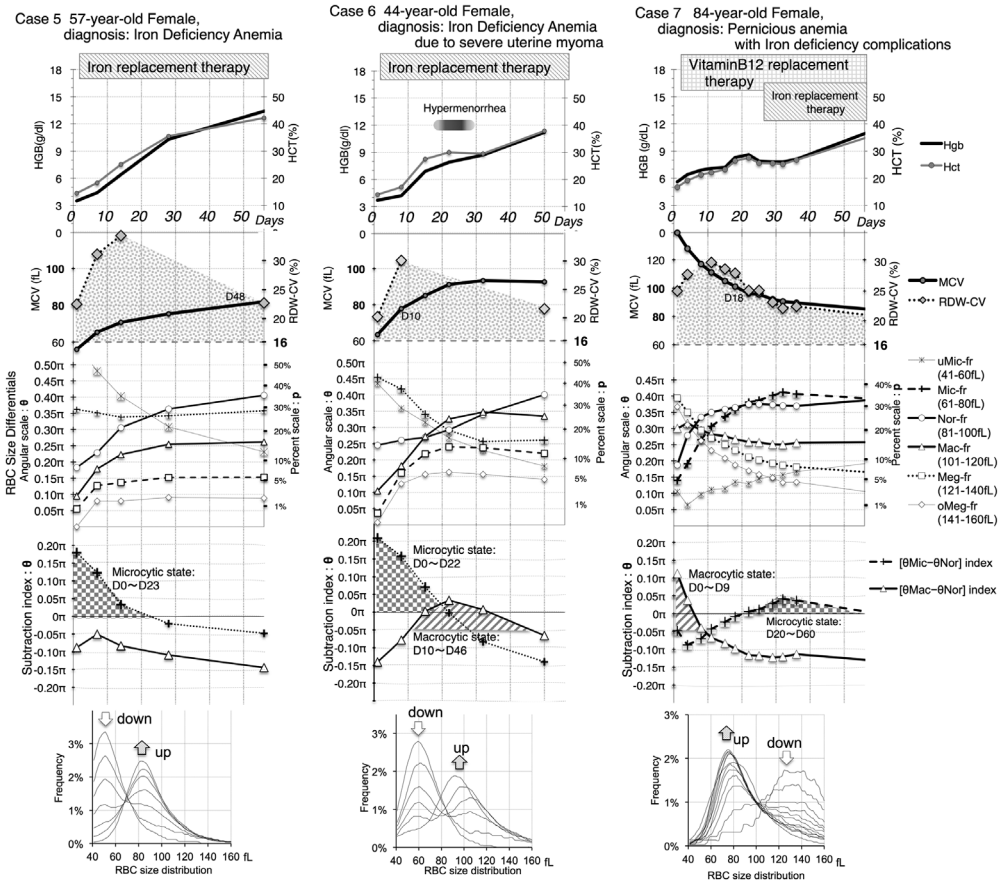

Figure 4. Notes: Identification of time-series trends of iron deficiency states related to clinical events and treatments using the SF-3000 analyzer.

Clinical problem: Case 5 showed typical recovery from iron-deficiency anemia. However, in both Cases 6 and 7, retardation in the recovery of HGB and/or HCT was apparent by three weeks after the start of medication: the cause in Case 6 appeared to be severe menstrual bleeding; the cause in Case 7 appeared to be iron deficiency complications related to treatment for pernicious anemia. Main relevant results from the superimposed RBC size distributions: ["-fr"="fraction"]. Cases 5 and 6: Both cases exhibited a similarly decreasing microcytic fraction and increasing Nor-fr. However, only Case 6 exhibited an emerging peak in Mac-fr with a bimodal pattern in the RBC size distribution. Case 7: Concurrent with a decreasing megalocytic state (in which Meg-fr was dominant), an upward trend in not only Nor-fr but also Mic-fr was observed. Inferred Clinical Significance of Time-Series Differential Indices: The durations of the microcytic states of [θMic−θNor] > 0π in both Case 5 and Case 6 were similar at slightly more than three weeks after the start of medication, but the transient macrocytic state of [θMac−θNor] > −0.05π in Case 6, which suggests a response of excessive erythropoiesis to massive bleeding, might have caused the very early recovery in MCV value. In Case 7, the microcytic state might reflect the extent of iron deficiency, and the prior progressing trend toward a microcytic state might help guide the timing/need for ferric treatment to occur at least one week earlier than conducted for Case 7.

time-series trends would output: true pathological change + systematic error + random error. Therefore, if random error propagation can be statistically controlled according to our linearization method, our suggested graphical approach might, in some cases, potentially reveal hidden systematic error through sudden disturbances in otherwise constant trends as typical graphical patterns (see Figure 1). Examples of in vitro systematic error, appearing as a rightward or leftward shift in RBC size distribution, include irregular RBC swelling due to differences in osmotic pressure between plasma with hyperglycemia and the relatively hypotonic counting medium (Strauchen et al., 1981) or cellular membrane abnormalities. Thus, the instability of accuracy in RBC size differentials might occur easily and consequently affect uncertainty propagation in the subtraction index, as shown in Figure 1. It would therefore be necessary to evaluate time-series changes that may include fluctuating systematic error using precision-stabilized semi-*Angit*(p) plotting graphs.

4.4. Practical approach to evaluate clinical trends in RBC size differentials

We identified early therapeutic responses based on RBC size differentials, which enabled the evaluation of microcytic and macrocytic changes independently. This ability was particularly relevant for anisocytotic bimodal distributions, in which the MCV value may be within the normal range (80–100 fL) and RDW might become incalculable, as shown in Case 2 and Cases 5–7. The latent bimodal distributions apparent in these cases suggest that RBC size differentials (1) may help guide the timing or decision for additional treatments; and (2) may enable detailed monitoring of secondary RBC size abnormalities caused by inflammatory and circulatory disorders. As an example of typical use in microcytic anemias, the initial therapeutic response could be monitored based on the decreasing [θMic−θNor] index as an effect of ferric treatment, whereas an increase in the [θMic−θNor] index might indicate recurrence of iron deficiency.

4.5. Limitation and future areas of study

Uncertainty propagation in the subtraction index of RBC size differentials will always change erratically according to slight instability in the accuracy of the count ratio index, which might be caused by the fixed gating method of six fractions in RBC size distribution against adjustable gating in WBC differentials. However, quantitative monitoring with subtraction indices, such as the [θMic−θNor] and [θMac−θNor] indices, might have a significant advantage over objective evaluation of various degrees of anisocytosis from latent levels to overt levels. Therefore, by means of precision-stabilized semi-*Angit*(p) plotting graphs, we must investigate the clinical trends in each differential index's lines and simultaneously assess the influence of the instability of accuracy using typical pattern recognition, as above. Additionally, because elevated RDW has recently been investigated as a predictor of mortality in various non-hematological disorders (Cauthen et al., 2012; Hu et al., 2013; Lippi & Plebani, 2014; Montagnana et al., 2012), the RBC size differential method might offer greater RDW-related detail over the clinical courses of cases with poor prognoses. In our view, such cases might be associated with pathological rebalancing between RBC supply and RBC lifespan. Therefore, we hope to investigate these possibilities further via real-time integration of the size differential-time course analysis program into our routine practice to evaluate the initial hematological responsivity under various therapies (Price et al., 2011).

5. Conclusion

This study demonstrates that a clinical monitoring method using time-series RBC size differentials, with measurement precision standardized for reliable difference comparisons, can offer the following advantages: a more detailed RBC size distribution examination complementing the MCV and RDW indicators; an easily visualized, improved representation of anemic disorder treatment; and the possibility of indicating time-series rebalances in daily RBC supply vs. mean RBC age for each size fraction.

Acknowledgments

We express our thanks to professor Yoshiyuki Yamashita, Department of Information Science at Saga University; and Dr Takashi Kanematsu, Director of Nagasaki Harbor Medical Center City Hospital, for their constant support of this study.

Funding

The authors received no direct funding for this research.

Competing Interests

The authors declare no competing interest.

Author details

Sunao Atogami[1,2]
E-mail: atogami@hospital.sasebo.nagasaki.jp
Charles de Kerckhove[3]
E-mail: d_charles@ncho.jp
Katsunori Yanagihara[1]
E-mail: k-yanagi@nagasaki-u.ac.jp
Shimeru Kamihira[1,3]
E-mail: kamihira@nag.bbiq.jp

[1] Department of Laboratory Medicine, Nagasaki University Graduate School of Biomedical Sciences, 1-7-1, Sakamoto, Nagasaki-shi, Nagasaki 852-8501, Japan.
[2] Department of Laboratory Medicine, Sasebo City General Hospital, 9-3, Hirase-cho, Sasebo-shi, Nagasaki 857-8511, Japan.
[3] Translational Unit, Innovation and Translational Research Center (ITREC), Nagasaki Harbor Medical Center City Hospital, 6-39, Shinchimachi, Nagasaki-shi, Nagasaki 850-8555, Japan.

Citation information

Cite this article as: Red blood cell size differential method for time-series detailed monitoring of anemic disorders with RBC size abnormalities in mean corpuscular volume (MCV) and/or red blood cell distribution width (RDW), Sunao Atogami, Charles de Kerckhove, Katsunori Yanagihara & Shimeru Kamihira, Cogent Medicine (2016), 3: 1251833.

References

Cauthen, C. A., Tong, W., Jain, A., & Tang, W. H. (2012). Progressive rise in red cell distribution width is associated with disease progression in ambulatory patients with chronic heart failure. *Journal of Cardiac Failure, 18*, 146–152. doi:10.1016/j.cardfail.2011.10.013

Cohen, R. M., Franco, R. S., Khera, P. K., Smith, E. P., Lindsell, C. J., Ciraolo, P. J., ... Joiner, C. H. (2008). Red cell life span heterogeneity in hematologically normal people is sufficient to alter HbA1c. *Blood, 112*, 4284–4291. doi:10.1182/blood-2008-04-154112

Erslev, A. J., & Beutler, E. (1995). Production and destruction of erythrocytes. In E. Beutler, M. A. Lichtman, B. S. Coller, & T. J. Kipps (Eds.), *Williams hematology* (5th ed., pp. 425–441). New York, NY: McGraw-Hill.

Franco, R. S. (2012). Measurement of red cell lifespan and aging. *Transfusion medicine and hemotherapy, 39*, 302–307. doi:10.1159/000342232

Hajian-Tilaki, K. (2013). Receiver operating characteristic (ROC) curve analysis for medical diagnostic test evaluation. *Caspian Journal of Internal Medicine, 4*, 627–635.

Hu, Z., Sun, Y., Wang, Q., Han, Z., Huang, Y., Liu, X., ... Deng, A. (2013). Red blood cell distribution width is a potential prognostic index for liver disease. *Clinical Chemistry and Laboratory Medicine, 51*, 1403–1408. doi:10.1515/cclm-2012-0704

Kachel, V. (1982). Sizing of cells by the electrical resistance pulse technique. In N. Catsimpoolas (Ed.), *Cell analysis* (pp. 195–331). Boston, MA: Boston University School of Medicine, Plenum Press.

Kirk, R. E. (2013). *Experimental design: Procedures for the behavioral sciences*. Thousand Oaks, CA: Sage. http://dx.doi.org/10.4135/9781483384733

Lippi, G., & Plebani, M. (2014). Red blood cell distribution width (RDW) and human pathology. One size fits all. *Clinical Chemistry and Laboratory Medicine, 52*, 1247–1249. doi:10.1515/cclm-2014-0585

Montagnana, M., Cervellin, G., Meschi, T., & Lippi, G. (2012). The role of red blood cell distribution width in cardiovascular and thrombotic disorders. *Clinical Chemistry and Laboratory Medicine, 50*, 635–641. doi:10.1515/cclm.2011.831

Oehlert, G. W. (1992). A note on the delta method. *The American Statistician, 46*, 27–29. doi:10.1080/00031305.1992.10475842

Price, E. A., Mehra, R., Holmes, T. H., & Schrier, S. L. (2011). Anemia in older persons: Etiology and evaluation. *Blood Cells, Molecules, and Diseases, 46*, 159–165. doi:10.1016/j.bcmd.2010.11.004

Quigley, J. G., Means, R. T., & Glader, B. (2014). The birth, life, and death of red blood cells: erythropoiesis, the mature red blood cell, and cell destruction. In J. P. Greer, D. A. Arber, B. Glader, A. F. List, R. T. Means, Jr., F. Paraskevas, ... J. Foerster (Eds.), *Wintrobe's clinical hematology* (13th ed., pp. 83–124). Philadelphia, PA: Lippincott Williams & Wilkins.

Rezende, S. M., Lijfering, W. M., Rosendaal, F. R., & Cannegieter, S. C. (2014). Hematologic variables and venous thrombosis: Red cell distribution width and blood monocyte count are associated with an increased risk. *Haematologica, 99*, 194–200. doi:10.3324/haematol.2013.083840

Sacher, R. A., McPherson, R. A., & Campos, J. M. (1991). *Widmann's clinical interpretation of laboratory tests* (10th ed.). Philadelphia, PA: Davis Company.

Strauchen, J. A., Alston, W., Anderson, J., Gustafson, Z., & Fajardo, L. F. (1981). Inaccuracy in automated measurement of hematocrit and corpuscular indices in the presence of severe hyperglycemia. *Blood, 57*, 1065–1067.

Tatsumi, N., Tsuda, I., Furota, A., Takubo, T., Hayashi, M., & Matsumoto, H. (1999). Principle of blood cell counter–development of electric impedance method. *Sysmex Journal International, 9*, 8–20.

Taylor, J. R. (1997). *An introduction to error analysis: The study of uncertainties in physical measurements* (2nd ed.). Sausalito, CA: University Science Books.

Appendix 1

Procedures for data acquisition of RBC size distributions from PNG-format digital images

The probability distributions of each RBC size fraction were obtained by converting the PNG-format digital images output from the analyzer. After subdividing the x-axis into 256 points for compilation in a relational database, the y-value (frequency) of each corresponding x-value (fL) was determined by subtracting the reference height (shown in Figure A1 with red arrow) from the height to the bottom pixel of the volume distribution curve (shown in Figure A1 with green arrow). **Figure A1. How RBC size distributions are obtained from digital image data (Appendix 1).** Our method obtained data digitally using the XE-5000 analyzer's output PNG-formatted images. Figure A1 shows the x-axis composition of 256 pixels and how the y-value of each x-value is determined by 1) locating the pixel at the bottom of the volume distribution graph's light blue line (green arrow); and 2) finding the height difference between the green arrow and the reference red arrow.

Next, the zero-point for all RBC volume histograms was determined statistically by comparing the mean value calculated from all histograms with the corresponding mean value from all analyses reported for MCV by one-channel increments. This resulted in an origin shift to the right by 1 fL. All probability distribution-related calculations, from 41 to 160 fL, were performed again after zero-point adjustment and were once again compiled in a relational database such that each channel value was equivalent to the corresponding original femtoliter value.

Appendix 2

Induction of error variance stabilizing transformation for estimating the count ratio measurement uncertainties

The cytometric blood cell count method is considered random sampling without replacement, such that the cell count number x follows a hypergeometric distribution. Furthermore, if the measured total count number n is sufficiently large and constant, as is certainly the case, such a hypergeometric distribution can be approximated by the simpler binomial distribution.

Thus, for the variance of cell count ratio p, the division of *x* by n can be expressed as follows:

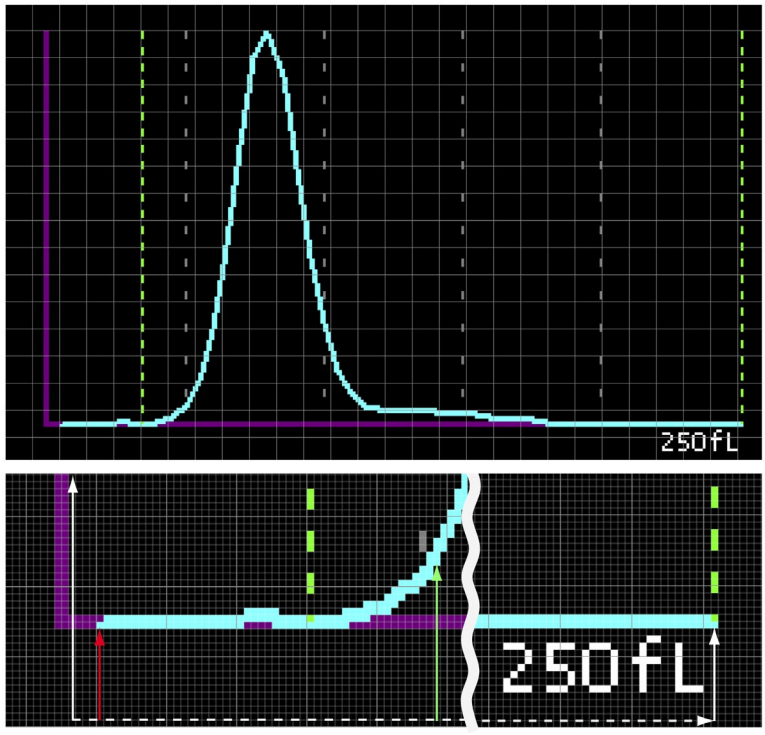

Figure A1. How RBC size distributions are obtained from digital image data (Appendix 1).

Notes: Our method obtained data digitally using the XE-5000 analyzer's output PNG-formatted images. Figure A1 shows the x-axis composition of 256 pixels and how the y-value of each x-value is determined by 1) locating the pixel at the bottom of the volume distribution graph's light blue line (green arrow); and 2) finding the height difference between the green arrow and the reference red arrow.

$$\frac{\mathrm{p}(1-\mathrm{p})}{n}$$

If the true value and the uncertainty of the measured value of count ratio p are represented as $\dot{\mathrm{p}}$ and $\delta\mathrm{p}$, respectively:

$$V[\mathrm{p}] = V\left[\dot{\mathrm{p}} + \delta\mathrm{p}\right] = V\left[\dot{\mathrm{p}}\right] + V\left[\delta\mathrm{p}\right] = V\left[\delta\mathrm{p}\right] = \frac{\mathrm{p}(1-\mathrm{p})}{n}$$

Here, a Taylor series expansion yields the linear approximate equation:

$$f(\mathrm{p}) = f(\dot{\mathrm{p}} + \delta\mathrm{p}) \approx f(\dot{\mathrm{p}}) + f'(\dot{\mathrm{p}}) \cdot \delta\mathrm{p}$$

Next, according to the "Delta method" (Oehlert, 1992), taking the variance of both sides yields the following:

$$V\left[f(\mathrm{p})\right] \approx V\left[f(\dot{\mathrm{p}}) + f'(\dot{\mathrm{p}}) \cdot \delta\mathrm{p}\right] = V\left[f(\dot{\mathrm{p}})\right] + \left(f'(\dot{\mathrm{p}})\right)^2 \cdot V\left[\delta\mathrm{p}\right] = \left(f'(\dot{\mathrm{p}})\right)^2 \cdot \frac{\mathrm{p}(1-\mathrm{p})}{n}$$

Next, the error variance stabilizing function $f(\mathrm{p})$, which estimates

$V\left[f(\mathrm{p})\right] = \mathrm{Const}$, is given by the following:

$$f'(\dot{\mathrm{p}}) = \sqrt{\frac{\mathrm{Const} \cdot n}{\mathrm{p}(1-\mathrm{p})}} \approx f'(\mathrm{p})$$

$$f(\mathrm{p}) = \sqrt{\mathrm{Const} \cdot n} \cdot \int_0^{\mathrm{p}} \frac{\mathrm{du}}{\sqrt{\mathrm{u}(1-\mathrm{u})}} = 2\sqrt{\mathrm{Const} \cdot n} \cdot \arcsin\sqrt{\mathrm{p}}$$

Thus, given that the total count number n is constant, we can conclude the following:

$$f(\mathrm{p}) = 2 \cdot \arcsin\sqrt{\mathrm{p}}$$

In contrast to the *Logit* function used in logistic analysis, we call this function *Angit*(p), with the transformed value defined as the angle ratio θ, as below:

$$\theta = \mathit{Angit}(\mathrm{p}) = 2 \cdot \arcsin\sqrt{\mathrm{p}},$$

where the value of the angle ratio θ varies from 0 to π such that we define the unit of angle ratio θ as π and set the range of variable θ as simply 0 to 1.

Appendix 3

The propagation of uncertainty in angular transformation vs. Logit transformation

The variance of the count ratio p, expressed as *V*[dp], is equal to $\frac{\mathrm{p}(1-\mathrm{p})}{n}$

because the cytometric RBC count ratio p can be approximated as a binomial distribution, where the total count number *n* is constant.

Based on the relationship $\mathrm{d}\mathit{Angit}(\mathrm{p}) = \frac{dp}{\sqrt{\mathrm{p}(1-\mathrm{p})}}$ and substituting $\frac{\mathrm{p}(1-\mathrm{p})}{n}$ for *V*[dp],

the error variance of *Angit*(p) with angle ratio θ is estimated as below:

$$V\left[\mathit{Angit}(\mathrm{p})\right] = V\left[\mathrm{d}\mathit{Angit}(\mathrm{p})\right] = V\left[\frac{\mathrm{dp}}{\sqrt{\mathrm{p}(1-\mathrm{p})}}\right] = \frac{1}{\mathrm{p}(1-\mathrm{p})} \cdot V\left[\mathrm{dp}\right] = \frac{1}{\mathrm{p}(1-\mathrm{p})} \cdot \frac{\mathrm{p}(1-\mathrm{p})}{n} = \frac{1}{n}$$

Conclusion: The error variance of *Angit*(p) is not affected by the quantity of the count ratio p and thus is constant.

The error variance of *Logit*(p) is estimated as below, with the same *V*[dp] substitution as above:

$$V\left[\mathit{Logit}(\mathrm{p})\right] = V\left[\mathrm{d}\mathit{Logit}(\mathrm{p})\right] = V\left[\frac{dp}{\mathrm{p}(1-\mathrm{p})}\right] = \left(\frac{1}{\mathrm{p}(1-\mathrm{p})}\right)^2 \cdot V\left[dp\right] = \left(\frac{1}{\mathrm{p}(1-\mathrm{p})}\right)^2 \cdot \frac{\mathrm{p}(1-\mathrm{p})}{n} = \frac{1}{n\mathrm{p}(1-p)}$$

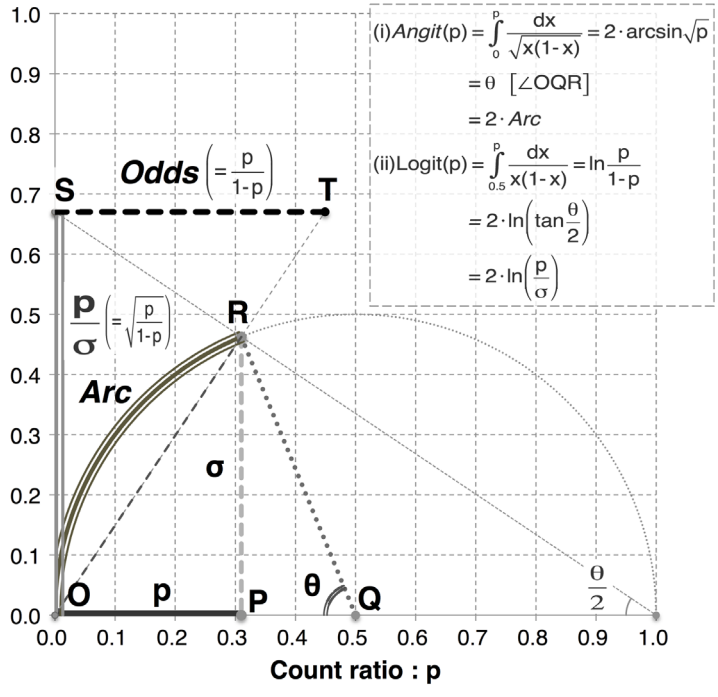

Figure A2. Geometric relationships between the *Angit* transformation and Logit transformation shown in a semicircular model.

Notes: The diagram above shows the geometric relationships among count ratio p, *Angit*(p) and Logit(p) based on the assumption of Bernoulli trials with the variance $\sigma^2 = \mathrm{p}(1\text{-}\mathrm{p})$.*1. Angit*(p) = twice the length of arc OR(*Arc*) = θ2. Logit(p) = twice the natural log of line segment OS(p/σ)Thus, *Angit*(p) indicates the standardization of the difference in probability p using *Arc*; by contrast, Logit(p) indicates the standardization of the relative ratio in likelihood p/σ using the natural log of p/σ.

***Conclusion*:** The error variance of Logit(p) can be near-stable in a p range such as [0.2, 0.8]; however, it is clear from the denominator alone that the instability is very high as p approaches 0 or 1.

As transformations of the same input variable, the *Angit*(p) and Logit(p) functions can be visualized and compared geometrically as well (see Figure A2). In the evaluation of cell count data by flow cytometry, it would be important to apply these transformations properly; *Angit*(p) appears applicable to the entire range of p for a precision-stabilized scale that is linear, whereas Logit(p) appears to be a useful linear-like operator only within an approximate p range of 0.2–0.8. **Figure A2. Geometric relationships between the *Angit* transformation and Logit transformation shown in a semicircular model.** The diagram above shows the geometric relationships among count ratio p, *Angit*(p) and Logit(p) based on the assumption of Bernoulli trials with the variance σ^2=p(1-p).*1. Angit*(p) = twice the length of arc OR(*Arc*) = $\theta 2$. Logit(p) = twice the natural log of line segment OS(p/σ)Thus, *Angit*(p) indicates the standardization of the difference in probability p using *Arc*; by contrast, Logit(p) indicates the standardization of the relative ratio in likelihood p/σ using the natural log of p/σ.

***Cogent Medicine* (ISSN: 2331-205X) is published by Cogent OA, part of Taylor & Francis Group.**